

Measuring the plasma-wall charge by infrared spectroscopy

K. Rasek, F. X. Bronold, and H. Fehske

Institut für Physik, Universität Greifswald, 17487 Greifswald, Germany

M. Bauer

*Institut für Experimentelle und Angewandte Physik,
Christian-Albrechts-Universität zu Kiel - 24098 Kiel, Germany*

(Dated: September 11, 2018)

We show that the charge accumulated by a dielectric plasma-facing solid can be measured by infrared spectroscopy. The approach utilizes a stack of materials supporting a surface plasmon resonance in the infrared. For frequencies near the Berreman resonance of the layer facing the plasma the reflectivity dip—measured from the back of the stack, not in contact with the plasma—depends strongly on the angle of incidence making it an ideal sensor for the changes of the layer’s dielectric function due to the polarizability of the trapped surplus charges. The charge-induced shifts of the dip, both as a function of the angle and the frequency of the incident infrared light, are large enough to be measurable by attenuated total reflection setups.

I. INTRODUCTION

Fundamental to any interface is charge separation. This universal mantra holds also for solids facing an ionized gas where an electron-depleted region in front of the solid is balanced by an electron-rich region inside or on top of the solid depending on the solid’s electronic structure. The electron-depleted, positive part of the double layer—the plasma sheath—has been studied rather extensively in the past, in particular, its merging with the bulk plasma^{1–3}. But the negative part—the wall charge—and its merging with the bulk of the solid received little attention⁴, although it is an integral part of the electric response of the plasma-solid interface and thus unavoidably linked to the overall charge balance of the discharge. Especially the behavior of microdischarges integrated on semiconducting substrates^{5,6} may be strongly affected by the charge dynamics inside the substrate. However, to develop an understanding of it requires experimental techniques probing inside the solid. So far only a few attempts have been made to measure the charge accumulated by a solid in contact with a plasma. Besides traditional electric probes⁷ and micron-size opto-mechanical charge sensors⁸, which both utilize the principle of electric influence, the opto-electric Pockels effect⁹ has been used for that purpose. The latter was developed into a rather sophisticated tool for lateral imaging of the wall charge in barrier discharges¹⁰. It works however only for dielectric coatings featuring the Pockels effect. For the dielectrics typically used in low-temperature plasma physics—SiO₂ and Al₂O₃—it is not applicable. The semiconductors hosting the arrays of microdischarges referred to above are also not Pockels-active.

In this work we propose an infrared diagnostics for the charge collected by plasma-facing dielectrics which also works for the standard materials used in plasma physics. It utilizes the charge-sensitivity of the infrared reflectivity of a layered structure in contact with a plasma, where the plasma-facing, charge-collecting layer is made out of the dielectric of interest. Its width is chosen such

that it supports a Berreman mode¹¹, thereby making the device sensitive to the low charge densities expected at plasma-solid interfaces compared to the rather high densities at solid-electrolyte interfaces^{12,13} and semiconductor surfaces^{14,15}, to which such an arrangement could be also applied. Using an attenuated total reflection (ATR) spectroscopy setup enables us to utilize as a charge diagnostics not only the charge-sensitive frequency shift of the Berreman mode but also the shift of the angle of incidence where the mode occurs.

The stack of materials comprising the measuring device, which we envisage to be inserted into the plasma wall or the electrode, is shown in fig. 1. Due to the metal layer and the optical prism on top of it surface plasmon polaritons (SPPs) are excited which—by avoided resonance crossing with the Berreman mode of the layer facing the plasma and consisting of the material of interest—cause a strong dependence of the reflectivity of the stack on the angle of incidence. If one is interested only in measuring the total charge collected by the dielectric the charge can be confined to a narrow region using a rather thin plasma-facing layer separated from the metal by a dielectric with negative electron affinity producing thereby a potential well. In case the density profile normal to the interface should also be mapped out, the plasma-facing layer has to be thick enough to host the profile yet thin enough to still support the Berreman resonance.

To demonstrate the feasibility of the proposal we calculate the reflectivity of the structure shown in fig. 1 as a function of the angle of incidence and the wavenumber (which we use in the final plots instead of the frequency) of the incident electromagnetic wave assuming—for simplicity—the surplus charges distributed homogeneously in the plasma-facing layer. The surplus charges’ polarizability, which we obtain from a memory function approach taking electron-phonon scattering into account¹⁶, modifies the dielectric function of the layer and is the ultimate reason for the charge-induced shifts of the Berreman mode. In the infrared the shifts we obtain are

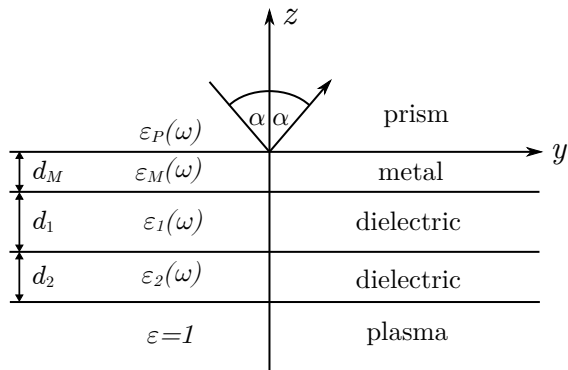


FIG. 1. Structural composition of the system under consideration. The prism and metal layer allow plasmon resonance. The dielectric materials are chosen so that the surplus charges are confined to the plasma-facing layer, which is the material of interest.

large enough to be detectable with common reflectivity setups. For the proof of principle presented in this work we focus on measuring the total charge and not the whole density profile. It would require a more sophisticated theoretical treatment, taking nonlocal surface effects of the electromagnetic response of the charged stack into account, and is left for future work. The widths of the layers can thus be used almost freely as parameters to optimize the sensitivity of the setup.

II. THEORETICAL DESCRIPTION

The physical process enabling the structure shown in fig. 1 to be used as a charge sensing device is the interaction of the surface plasmon resonance (SPR) of the metallic layer below the prism and the Berreman mode of the plasma-facing, charge-carrying dielectric layer. To identify suitable materials to be stacked together we start the description of our proposal with a discussion of the role of each layer. The prism and the metallic layer are essential for the SPR. They constitute a Kretschmann configuration¹⁷, where total reflection of the incident wave at the prism-metal interface creates the evanescent wave necessary for exciting a SPP at the metal-dielectric interface¹⁸. For SPR the wave extending into the plasma needs to be evanescent as well. Hence, the total reflection condition $\sin^2 \alpha > 1/\epsilon_P$ imposes a lower limit to the angle of incidence, depending on the prism material. Because of this relation, the dielectric function of the prism should be nearly independent of frequency ω in the range of interest. In addition it should be real and positive. In the exploratory calculation presented below we use KBr, a material commonly used in infrared optics because of its transparency in that frequency range¹⁹. Its dielectric function varies little in the relevant frequency range, but the critical angle already depends significantly on frequency. The only condition for the metal layer is a large negative real and a nonvanishing imaginary part of the

dielectric function for infrared frequencies. A common material choice for SPR is gold. We found a thickness of the gold film around 10nm to be optimal for our purpose. It is smaller than the 50nm typically used in optical SPR¹⁸.

The actual plasma wall of interest is the plasma-facing layer. Separated from the metal by another dielectric layer, it is made out of the material whose charge accumulation properties one wants to study. Since the dielectrics commonly used in plasma physics are electro-positive, and these are the ones we are aiming at, adding a separation layer with negative electron affinity confines the surplus electrons collected from the plasma to the plasma-facing layer. The separating (insulating) layer also prevents the surplus electrons from spilling into the metal layer. Since in this work we focus on determining the total amount of charge collected by the material in contact with the plasma, it is advantageous to make the plasma-facing layer rather thin. The insulating layer, preventing the surplus electrons from leaving the film, leads then to a high local space charge density and thus to a high polarizability modifying the dielectric function of the film. It is this modification that makes the reflectivity of the stack charge-sensitive. We found a thickness of $d_2 = 20$ nm to give satisfactory results. In our simulations Al_2O_3 is used as the plasma-facing material, but other electro-positive dielectrics, such as SiO_2 , could be used as well. The thickness of the insulating layer is not critical. We choose $d_1 = 40$ nm, but even much thicker layers would not change the results significantly (see discussion below). For the material there are little restrictions. However, it is convenient if the infrared resonances of this layer are well separated from the resonances of the plasma-facing layer. We use MgO. Since the densities of ions and electrons in the plasma are extremely low, the plasma is treated like a vacuum, that is, its dielectric function $\epsilon = 1$.

We investigate the reflectivity, that is, the ratio of the incident and reflected beam intensities as a function of the angle of incidence and the frequency of the impinging infrared light. As usual, only p-polarized light is able to excite SPPs¹⁸. Using the method of Lambin *et al.* for multilayered materials^{20,21}, the solution of the Maxwell equations yields an effective dielectric function $\xi_0(k, \omega)$ that can be written as a continued fraction,

$$\xi_0(k, \omega) = a_1 - \frac{b_1^2}{a_1 + a_2 - \frac{b_2^2}{a_2 + a_3 - \dots}} \quad (1)$$

with

$$a_i = \frac{\epsilon_i}{\sqrt{1 - \left(\frac{\omega}{kc}\right)^2 \epsilon_i} \tanh\left(\sqrt{1 - \left(\frac{\omega}{kc}\right)^2 \epsilon_i} kd_i\right)} \quad (2)$$

and b_i the same as a_i when replacing \tanh by \sinh . Here $k = \omega/c\sqrt{\epsilon_P} \sin \alpha$ is the y -component of the wave vector which is conserved throughout the system, ϵ_i is the

(ω dependent) dielectric function in layer i , d_i is the layer's thickness and c is the vacuum speed of light. For the semi-infinite plasma layer the coefficients are $a_4 = 1/\sqrt{1 - (\omega/(kc))^2}$ and $b_4 = 0$. The value ξ_0 is the solution of a Riccati equation at the prism-metal-interface, that is at $z = 0$ (see fig. 1), and determines the reflectivity of the system via

$$|R|^2 = \left| \frac{\xi_0 - i\varepsilon_P \tan \alpha}{\xi_0 + i\varepsilon_P \tan \alpha} \right|^2. \quad (3)$$

For the full derivation see ref.²¹, where the calculation is given without the prism, but the adjustments to account for it are fairly simple.

In the infrared, the dielectric functions are highly frequency dependent. Most dielectric materials can be modeled as a system of damped oscillators, so that the real and imaginary part of the dielectric function, labeled ε' and ε'' respectively, can be calculated as

$$\varepsilon'(\omega) = \varepsilon_\infty + \sum_i \frac{f_i \omega_i^2 (\omega_i^2 - \omega^2)}{(\omega_i^2 - \omega^2)^2 + \gamma_i^2 \omega^2} \quad (4)$$

and

$$\varepsilon''(\omega) = \sum_i \frac{f_i \omega_i^2 \gamma_i \omega}{(\omega_i^2 - \omega^2)^2 + \gamma_i^2 \omega^2}. \quad (5)$$

The values for the resonance frequencies ω_i , the weighing factors f_i , the damping coefficients γ_i , and the limit values ε_∞ are given in table I for MgO and Al₂O₃. For the gold layer, values from ref.²⁴ were used and when necessary interpolated. In the infrared the absolute value of both real and imaginary part are large (> 1000), the real part being negative, and show roughly a ω^{-2} proportionality. The dielectric function of KBr is given as a Sellmeier equation and converted to the form of eq. (4) for convenience, but no imaginary part is considered.

Analyzing eqs. (1) - (3), it becomes clear that the reflectivity $|R|^2$ will be unity if the dielectric functions have no imaginary parts, because then ξ_0 is real as well. Although the dielectric function of gold has a significant imaginary part in the whole infrared range, it only partakes in the absorption process through the surface plasmon. If the plasmon dispersion relation is not met, there is no absorption by the gold layer. Taking the bulk dielectric function of Al₂O₃—the material of interest we use as an illustration—plotted in fig. 2 into consideration, absorption frequencies can be identified. They are independent of the angle of incidence and occur where the imaginary part of the dielectric function is considerable compared to the real part, that is, at the resonance frequencies ω_i , or where the real part crosses or approaches zero while the imaginary part stays finite, as it is the case near $\lambda^{-1} = 900\text{cm}^{-1}$. At this particular wavenumber, an enhanced absorption occurs for a film whose thickness

TABLE I. Material parameters for the dielectric functions of MgO²², Al₂O₃²³ and KBr¹⁹.

	MgO	Al ₂ O ₃	KBr
ε_∞	3.01	3.2	1.39408
$\omega_1(\text{cm}^{-1})$	401	385	114.00
f_1	6.6	0.3	2.06217
$\gamma_1(\text{cm}^{-1})$	7.619	5.58	0
$\omega_2(\text{cm}^{-1})$	640	442	164.99
f_2	0.045	2.7	0.17673
$\gamma_2(\text{cm}^{-1})$	102.4	4.42	0
$\omega_3(\text{cm}^{-1})$		569	53476
f_3		3.0	0.15587
$\gamma_3(\text{cm}^{-1})$		11.38	0
$\omega_4(\text{cm}^{-1})$		635	57803
f_4		0.3	0.01981
$\gamma_4(\text{cm}^{-1})$		12.7	0
$\omega_5(\text{cm}^{-1})$			68493
f_5			0.79221
$\gamma_5(\text{cm}^{-1})$			0
m^*/m		0.4	

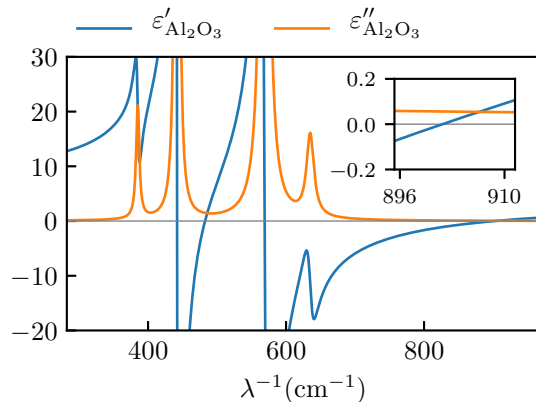


FIG. 2. Bulk dielectric function of Al₂O₃ obtained from eqs. (4) and (5) using the parameters given in table I. Absorption resonances occur when the imaginary part of the dielectric function is large. The zero crossing of the real part at about $\lambda^{-1} = 900\text{cm}^{-1}$ (see inset) will give rise to a Berreman resonance in a film of thickness much smaller than the corresponding wavelength¹¹. It is the mode we use for charge detection. Other resonances occur at lower wavenumbers, but are significantly weaker and thus unsuitable for our purpose.

is much smaller than the corresponding wavelength. In the infrared the film can be as thick as a few hundred nanometers for the resonance—which is called Berreman resonance¹¹—to occur. It turns out to be very charge-sensitive and thus most suitable for our purpose because the additional polarizability in the film due to the surplus

charges leads to a strong shift of the Berreman resonance.

The polarizability $\alpha_P = 4\pi i\sigma_b/\omega$, which is added to the dielectric function of the plasma-facing layer, is caused by the charges deposited into the plasma-facing layer. Using the memory function approach of ref.¹⁶, the bulk conductivity σ_b determining α_P can be calculated as

$$\sigma_b(\omega) = \frac{e^2 n_b}{m^*} \frac{1}{\omega + M(\omega)}, \quad (6)$$

where e and m^* are the electron charge and conduction band effective mass, and n_b is the bulk density of the surplus electrons. The memory function $M(\omega)$ takes electron-phonon scattering into account via the interaction Hamiltonian $H_{\text{int}} = \sum_{\mathbf{k}, \mathbf{q}} M c_{\mathbf{k}+\mathbf{q}}^\dagger c_{\mathbf{k}} (a_{\mathbf{q}} + a_{-\mathbf{q}}^\dagger)/(\sqrt{V}q)$, with $M = \sqrt{2\pi e^2 \hbar \omega_{\text{LO}} (\varepsilon_\infty^{-1} - \varepsilon_0^{-1})}$, where $a_{\mathbf{q}}^{(\dagger)}$ and $c_{\mathbf{k}}^{(\dagger)}$ are the annihilation (creation) operators of phonons and electrons, respectively, and V is the volume of the layer. To second order in M the memory function is given by

$$M(\omega) = M_0 \int_{-\infty}^{\infty} d\bar{\nu} \frac{j(-\bar{\nu}) - j(\bar{\nu})}{\bar{\nu}(\bar{\nu} - \nu - i0^+)} \quad (7)$$

with

$$j(\nu) = \frac{e^\delta}{e^\delta - 1} |\nu + 1| e^{-\delta(\nu+1)/2} K_1(\delta |\nu + 1|/2) + \frac{1}{e^\delta - 1} |\nu - 1| e^{-\delta(\nu-1)/2} K_1(\delta |\nu - 1|/2), \quad (8)$$

where $\nu = \omega/\omega_{\text{LO}}$ is the frequency in units of the longitudinal optical phonon frequency, $\delta = \hbar\omega_{\text{LO}}/(k_B T)$ is the LO phonon energy in units of the thermal energy (we use $T = 300\text{K}$), K_1 is a modified Bessel function, the prefactor in eq. (7) is $M_0 = 4e^2 \sqrt{m^* \omega_{\text{LO}} \delta} (\varepsilon_\infty^{-1} - \varepsilon_0^{-1}) / (3\sqrt{(2\pi\hbar)^3})$, ε_0 is the static dielectric function, and $\omega_{\text{LO}} = 807\text{cm}^{-1}$ is a longitudinal optical phonon frequency¹⁶.

III. RESULTS

The reflectivity of the stack of materials without surplus charges is shown in fig. 3 as a function of the wavenumber λ^{-1} and the angle of incidence α . Since the dispersion of SPPs is below the one of regular light, SPR occurs in our setup only for angles larger than the critical angle $\alpha_c = \arcsin(1/\sqrt{\varepsilon_P})$ which is wavenumber dependent because of the wavenumber dependence of the prism's dielectric function (solid black line). The SPP dispersion is the relation between the wavenumber and the angle of incidence where absorption is observed. Because of the wavenumber dependence of α_c the dispersion is bent over to larger angles. When another

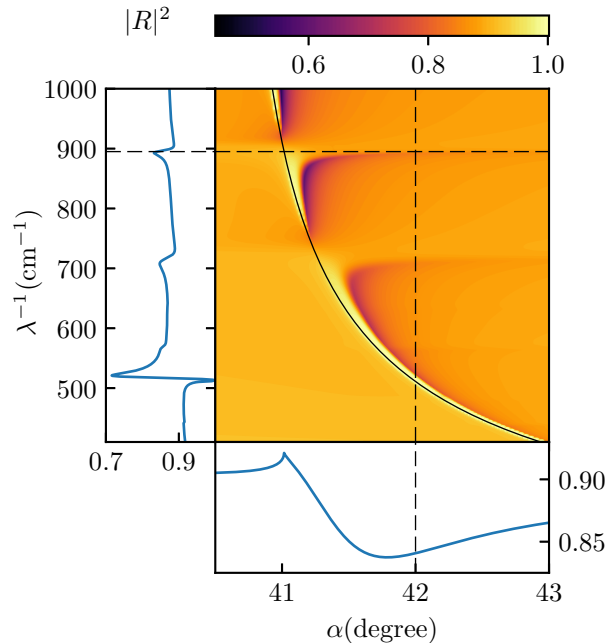


FIG. 3. Reflectivity of the uncharged stack as a function of the angle of incidence α and the wavenumber λ^{-1} . The parameters are $d_M = 10\text{nm}$, $d_1 = 40\text{nm}$ and $d_2 = 20\text{nm}$. On the left the reflectivity is shown as a function of λ^{-1} for a fixed angle of incidence $\alpha = 42^\circ$, indicated by the vertical dashed line, and on the bottom the reflectivity is plotted as a function of the angle of incidence for $\lambda^{-1} = 895\text{cm}^{-1}$, indicated by the horizontal dashed line. The solid black line gives the critical angle for each wavenumber. The top horizontal branch at about 900cm^{-1} is caused by the Berreman resonance of the Al_2O_3 layer, the lower one near 700cm^{-1} is the Berreman mode of the MgO layer, and the strong feature slightly above 500cm^{-1} is an ordinary SPR.

absorption mechanism occurs at the same wavenumber, like the Berreman resonance, avoided resonance crossing deforms the dispersion further, as can be seen for λ^{-1} around 900cm^{-1} and 700cm^{-1} . Far away from the critical angle, that is, far away from the black solid line, only the bulk absorption of the dielectric layers at these wavenumbers is observable and there is no angle dependence. However, approaching the critical angle, the horizontal absorption lines merge into the plasmon mode. Because the dispersion can be rather flat, when measuring the reflectivity as a function of the angle of incidence around these wavenumbers, a very broad minimum is observed compared to the narrow minimum resulting from the undisturbed plasmon dispersion. This broad minimum in the angle of incidence shown in the bottom panel of fig 3 for λ^{-1} around 900cm^{-1} is very sensitive to the wavenumbers. It will thus be modified when surplus charges change the dielectric function of the plasma-facing layer and hence the zero-crossing of its real part.

Two practical ways are thus possible to measure a

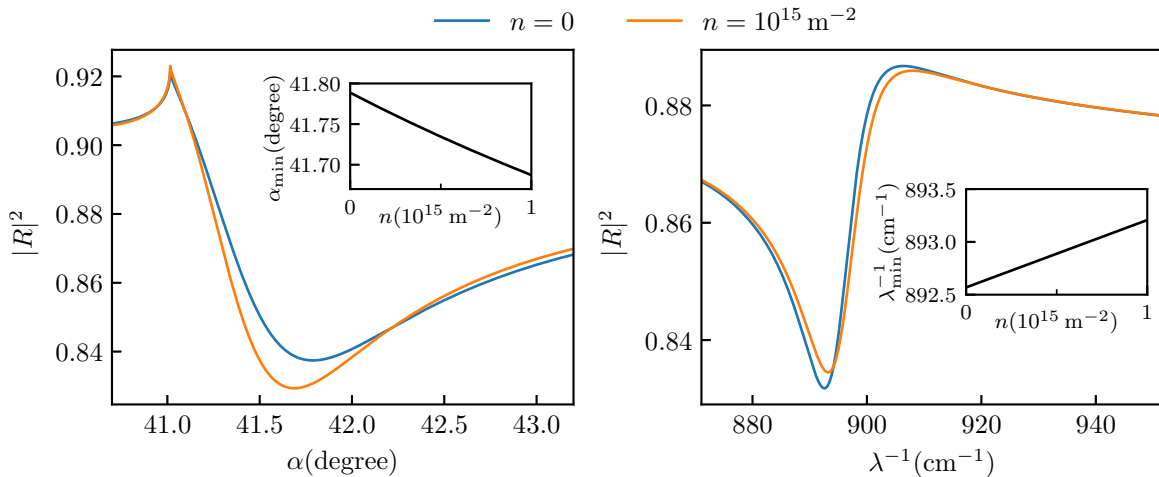


FIG. 4. Reflectivity for different surface charges. On the left it is shown as a function of the angle of incidence and $\lambda^{-1} = 895 \text{ cm}^{-1}$ while on the right it is plotted as a function of λ^{-1} and $\alpha = 42^\circ$. The insets show the minimum value of the dip as a function of the surface charge n , which is homogeneously distributed in the plasma-facing layer giving rise to a space charge density $n_b = n/d_2$. The parameters are the same as in fig. 3. The shifts at the maximum density $n = 10^{15} \text{ m}^{-2}$ are 0.1014° and 0.6377 cm^{-1} .

reflectivity curve in this type of setup. Either the wavenumber λ^{-1} of the incident laser is fixed and the reflectivity is measured as a function of the angle of incidence α , or the latter is fixed and the laser's wavenumber is varied. When surplus charges are added to the plasma-facing layer, the dispersion slightly changes because of the modification of the layer's dielectric function by the polarizability of the charges, and the dips in both measurement methods shift. As can be seen in fig. 4 typical values for these shifts are 0.1° in the angle and 0.6 cm^{-1} in the wavenumber—or 8 nm in the wavelength—for a surface charge density of $n = 10^{15} \text{ m}^{-2}$ which is a rough estimate of the charge density to be expected based on the charge of dust particles in a low-temperature neon discharge²⁵. These shifts should be measurable in common ATR setups which in the visible range achieve resolutions of about 10^{-3} degree or 0.1 nm. Refined setups provide even resolutions up to 10^{-5} degree or $5 \times 10^{-4} \text{ nm}$ ^{26,27}. From the measured shift we can then determine the surface charge n which for homogeneously distributed space charges obeys $n = n_b d_2$ with n_b the bulk density and d_2 the thickness of the plasma-facing layer. In the inset of fig. 4 we show how the minimum of the dips shifts as a function of the charge density. Measuring the position of the dip minimum opens thus a way to determine the surface charge n .

The shifts can be explained as follows: Considering that the additional charges shift the dielectric function linearly, and that the absorption mode occurs where the dielectric function crosses zero, it is quite clear that the surface charges will shift the dispersion upward in the vicinity of the Berreman mode. At a fixed wavenumber, the absorption dip as a function of the incident angle will

thus shift to a lower angle, while for a fixed angle the dip will move to a higher wavenumber by about as much as the zero crossing of the dielectric function is shifted. To maximize the shift of the minimum angle, the dispersion should be as flat as possible at the chosen wavenumber. On the other hand, since the absorption becomes weaker as λ^{-1} approaches the Berreman resonance, due to the avoided resonance crossing, the depth of the absorption dip is significantly reduced. Thus, one needs to balance between sensitivity and absorption strength when choosing the parameters. The data for the reflectivity dips and the charge-induced shifts of the reflection minimum shown in fig. 4 were obtained for a particular choice of parameters. However, especially the angular sensitivity can be significantly enhanced by other choices of parameters, as we will now discuss, but at the cost of flatter and broader absorption curves, that is, a decreased detectability.

In the rest of this section we describe the influence of the system parameters on the dispersion and the reflectivity curves shown in figs. 3 and 4. As mentioned above, the metallic layer is necessary for SPR, that is, for exciting SPPs. In the visible frequency range the optimal thickness d_M of the gold layer is about 50 nm. It is imposed by two effects. Too thick layers reduce SPP excitation by too much absorption in the metal, while too thin layers lead to too high radiation damping in the prism attenuating thereby also the SPR. In our case, the SPR creates a weak angle dependence of the reflectivity near the Berreman resonance, which is in the infrared. To be of any use as a charge diagnostics it has to be detectable. We have thus to ensure that the metal layer is not too thick for most of the infrared radiation to be

reflected at the prism-metal interface. Absorption by the SPPs or the modes of the dielectric bulk would then be too weak to produce a sizeable reflectivity dip. For a thickness of $d_M = 10\text{nm}$ we find about a 5 to 10% drop at the minimum (see figs. 3 and 4). If the layer is twice that thick the drop is only around 1 to 2%.

The insulating dielectric layer underneath the metal is not involved in the absorption process at the relevant wavenumbers, because the Berreman resonance affiliated with this material is at a lower wavenumber, see fig. 3. Moreover, at the considered wavenumbers and angles the electromagnetic wave propagates through the insulating layer. Thus, its thickness d_1 is more or less arbitrary. Even for $d_1 > 1\mu\text{m}$ the shifts of the Berreman mode of the plasma-facing layer are still present. Only the avoided resonance crossing of the Berreman mode of the insulating layer is somewhat suppressed. The particular numerical values of the shifts of the reflectivity dips, both in the angle of incidence and the wavenumber, vary with the thickness. For instance, for $d_1 = 1\mu\text{m}$ with the rest of the parameters as in fig. 3, the shifts for $n = 10^{15}\text{m}^{-2}$ are 0.142° and 0.386cm^{-1} , while for $d_1 = 4\mu\text{m}$ the shifts are 0.076° and 0.712cm^{-1} .

The thickness d_2 of the plasma-facing layer has—in the present case, where we want to measure only the total amount of surplus charge, and hence use the layer also for charge confinement—a significant influence on the charge sensitivity of the method. It affects both the reflectivity dip in angle and in wavenumber. The reason is quite obvious since we assume the total surface charge n provided by the plasma homogeneously distributed within that layer. Hence, the bulk charge density, entering the polarizability through the conductivity (6), is given by $n_b = n/d_2$. The thicker the plasma-facing layer the smaller is therefore n_b and hence the polarizability driving the shifts of the reflectivity minima. The larger d_2 the less pronounced is thus the reflectivity dip as a function of λ^{-1} for a fixed angle making it thus less suitable for charge diagnostics. However, in the setup we use a thicker layer implies also that the avoided resonance crossing becomes stronger, that is, the flat branch of the dispersion at around 900cm^{-1} (viz: fig. 3) degrades already at larger angles. As a result, the reflectivity dip as

a function of the angle becomes wider and less deep. But surprisingly it shifts stronger with the surface charge density n than the narrower dip of a less thick layer. Thus, by choosing the thickness d_2 accordingly, the charge sensitivity of the reflectivity dip as a function of angle for fixed λ^{-1} can be enhanced. Pushing the laser frequency closer to the Berreman resonance has the same effect. It makes the reflectivity dip flatter and wider but at the same time also more charge-sensitive.

IV. CONCLUSION

We showed that in an infrared ATR setup the presence of surplus charges deposited into a plasma-facing dielectric layer manifests itself in a shift of a reflectivity dip both in the wavenumber and the angle of incidence. The results we obtained suggest moreover that the shifts are detectable by standard infrared equipment. In this exploratory work we focused on detecting the total charge accumulated in the plasma-facing film which we moreover assumed to be homogeneously distributed. The thicknesses of the layers of the stack used as a charge measuring device could thus be chosen freely to optimize the dip's detectability and charge sensitivity. In principle the device can also be used to map out the density profile normal to the interface. The plasma-facing layer then has to be thick enough to host the whole space charge profile. More refined theoretical treatments are then necessary. The principle of the method however remains the same: Using the Berreman mode of the plasma-facing layer as a charge sensor. Compared to other approaches measuring the wall charge, the method we suggest does not exploit material-specific properties. Being a spectroscopic technique it may have the potential to track the charge accumulation in time. It does not require complex experimental setups. In fact we expect it to be compatible with commonly used discharge geometries. The stack of materials measuring the wall charge can be integrated into the plasma wall or the electrode. Mechanical stability is then provided by a sufficiently thick prism.

¹ R. P. Brinkmann, J. Phys. D: Appl. Phys. **42**, 194009 (2009).

² R. N. Franklin, J. Phys. D: Appl. Phys. **36**, R309 (2003).

³ K.-U. Riemann, J. Phys. D: Appl. Phys. **24**, 493 (1991).

⁴ F. X. Bronold and H. Fehske, J. Phys. D: Appl. Phys. **50**, 294003 (2017).

⁵ J. G. Eden, S.-J. Park, J. H. Cho, M. H. Kim, T. J. Houllahan, B. Li, E. S. Kim, T. L. Kim, S. K. Lee, K. S. Kim, J. K. Yoon, S. H. Sung, P. Sun, C. M. Herring, and C. J. Wagner, IEEE Trans. Plasma Sci. **41**, 661 (2013).

⁶ R. Dussart, L. J. Overzet, P. Lefauchaux, T. Dufour, M. Kulsreshath, M. A. Mandra, T. Tillocher, O. Aubry,

S. Dozias, P. Ranson, J. B. Lee, and M. Goeckner, Eur. Phys. J. D **60**, 601 (2010).

⁷ E. Kindel and R. Arndt, Beitr. Plasmaphysik **20**, 119 (1980).

⁸ K. Pangal, S. L. Firebaugh, and J. C. Sturm, Appl. Phys. Lett. **69**, 1471 (1996).

⁹ T. Kawasaki, T. Terashima, Y. Zhu, T. Takada, and T. Maeno, J. Phys. D: Appl. Phys. **27**, 1646 (1994).

¹⁰ R. Tschiersch, M. Bogaczyk, and H.-E. Wagner, J. Phys. D: Appl. Phys. **47**, 365204 (2014).

¹¹ D. W. Berreman, Phys. Rev. **130**, 2193 (1963).

¹² J.-N. Chazalviel, J. Electroanal. Chem. **509**, 108 (2001).

- ¹³ J. G. Gordon II and S. Ernst, Surf. Sci. **101**, 499 (1980).
- ¹⁴ T. Wijesinghe and M. Premaratne, Opt. Express **20**, 7151 (2012).
- ¹⁵ M. Janipour, I. B. Misirlioglu, and K. Sendur, Sci. Rep. **6**, 34071 (2016).
- ¹⁶ R. L. Heinisch, F. X. Bronold, and H. Fehske, Phys. Rev. Lett. **109**, 243903 (2012).
- ¹⁷ E. Kretschmann, Z. Physik **241**, 313 (1971).
- ¹⁸ R. P. H. Kooyman, in *Handbook of Surface Plasmon Resonance*, edited by R. B. M. Schasfoort and A. J. Tudos (The Royal Society of Chemistry, London, 2008) Chap. 2, p. 15.
- ¹⁹ H. H. Li, J. Phys. Chem. Ref. Data **5**, 329 (1976).
- ²⁰ P. Lambin, J. P. Vigneron, and A. A. Lucas, Phys. Rev. B **32**, 8203 (1985).
- ²¹ P. Lambin, J. P. Vigneron, A. A. Lucas, and A. Dereux, Phys. Scripta **35**, 343 (1987).
- ²² J. R. Jasperse and X. Y, Phys. Rev. **146**, 526 (1966).
- ²³ A. S. Barker, Phys. Rev. **132**, 1474 (1963).
- ²⁴ R. L. Olmon and X. Y, Phys. Rev. B **86**, 235147 (2012).
- ²⁵ S. A. Khrapak, S. V. Ratynskaia, A. V. Zobnin, A. D. Usachev, V. V. Yaroshenko, M. H. Thoma, M. Kretschmer, H. Hoefner, G. E. Morfill, O. F. Petrov, and V. E. Fortov, Phys. Rev. E **72**, 016406 (2005).
- ²⁶ N. J. Tao, S. Boussaad, W. L. Huang, R. A. Arechabaleta, and J. D'Agnese, Rev. Sci. Instr. **70**, 4656 (1999).
- ²⁷ M. J. Jory and X. Y, Meas. Sci. Technol. **6**, 1193 (1995).